Dramatic rock embrittlement by rising confining stress at triaxial compression; experimental results, brittleness criteria, embrittlement mechanism

Boris Tarasov

The University of Western Australia, 35 Stirling Highway, Crawley WA 6009 Australia

borist.tarasov@uwa.edu.au

Keywords: rock embrittlement, triaxial compression, brittleness criteria, shear rupture mechanism.

Abstract. It is generally accepted that rising confining stress σ_3 increases ductility of rocks subjected to triaxial compression, where $\sigma_1 > \sigma_2 = \sigma_3$. This paper demonstrates that, in contrast to relatively soft rocks, intact hard rocks failed in mode II can increase their brittleness dramatically (hundreds of times) with rising σ_3. The brittleness variation in this case follows a typical pattern of initially increasing, reaching a maximum and then ultimately decreasing. The harder the rock, the greater is the effect of embrittlement. A shear rupture mechanism discussed in the paper shows that the embrittlement results from reduction of friction within the rupture zone with rising confining stress. The paper proposes two new brittleness criteria allowing for the representation of rock brittleness at triaxial compression within the range from absolute brittleness to absolute ductility in the form of continuous, monotonic and unambiguous scale of brittleness.

Introduction

It is generally believed that rising confining stress σ_3 increases ductility of rocks subjected to triaxial compression $\sigma_1 > \sigma_2 = \sigma_3$. Figure 1 illustrates this type of rock behaviour. A set of stress-strain curves in Figure 1a was obtained on sandstone specimens tested at different levels of σ_3. Dotted lines in Figure 1b show schematically variation of the post-peak modulus $M = d\sigma/d\varepsilon_1$ with rising σ_3. Shaded area here represents the post-peak rupture energy for $\sigma_{3(3)}$. Such variation in M and in the post-peak rupture energy indicates the increase in ductility with rising σ_3.

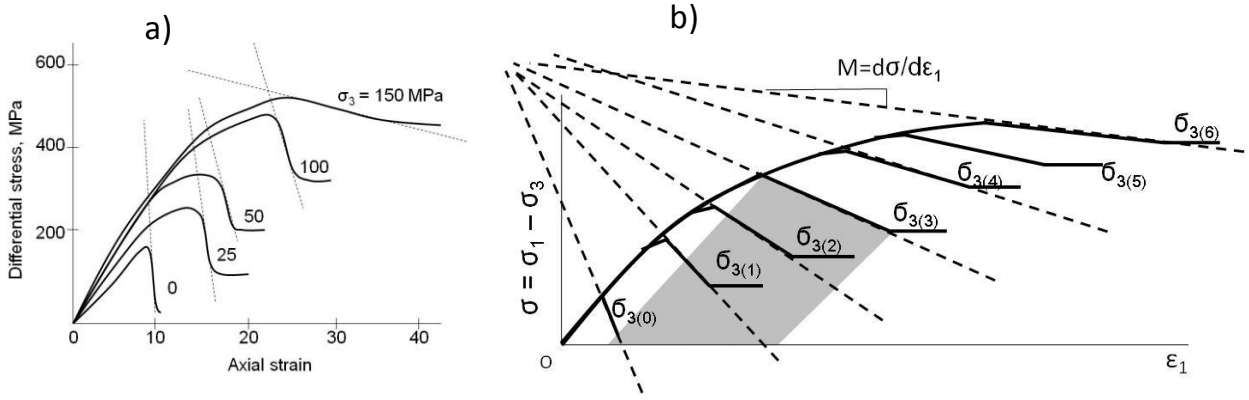

Fig.1. Commonly accepted rock behavior at different levels of confining stress σ_3. a) Stress-strain curves for sandstone. b) Schematic illustration of the post-peak modulus M variation with rising σ_3.

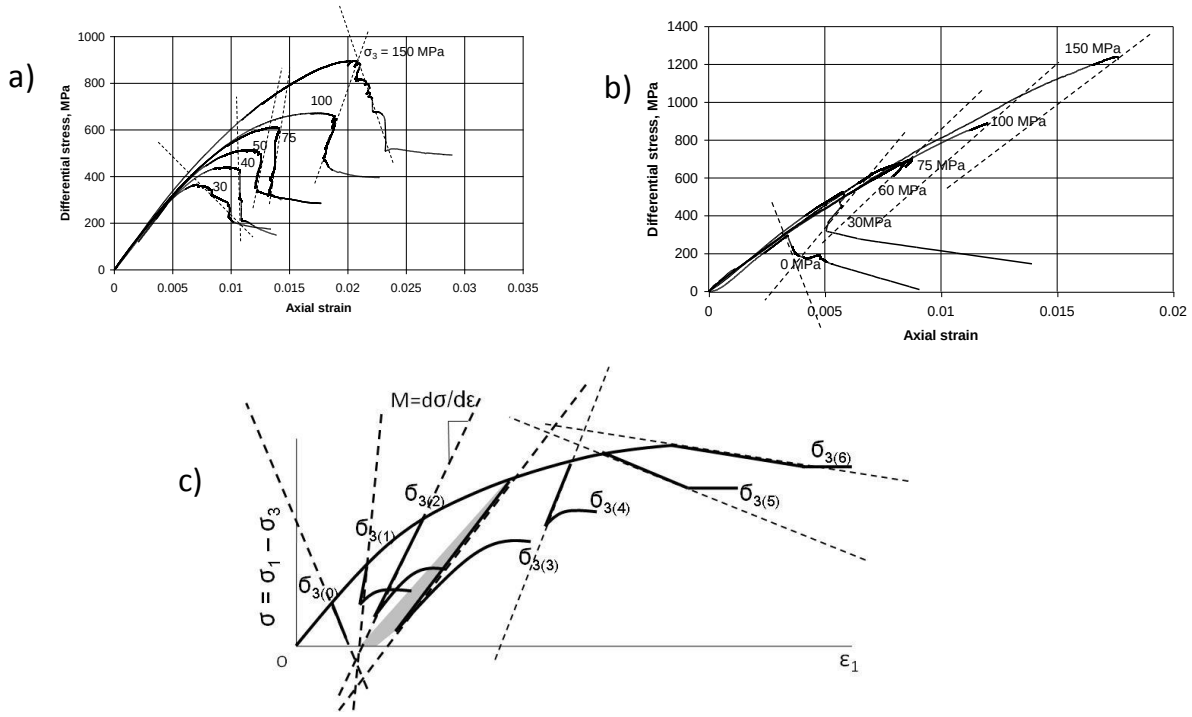

Fig.2. Unconventional behavior of hard rocks (quartzite – (a) and dolerite – (b)) with rising confining stress σ_3. c) Schematic illustration of the post-peak modulus M variation with rising σ_3.

Analysis of the post-peak behaviour of rocks of different hardness conducted in [1-3] demonstrates that, in contrast to soft rocks, hard rocks show unconventional behaviour with increasing confining stress σ_3. Figures 2a and 2b show experimental results obtained for quartzite and dolerite. Dotted lines in Figure 2c illustrate typical variation in the post-peak modulus M with rising σ_3 for such type of rocks. Shaded area here represents the post-peak rupture energy for $\sigma_{3(3)}$ curve. Within a certain rage of σ_3 the increase in σ_3 is accompanied by the contradirectional rotation of the dotted lines (post-peak characteristics) and by the decrease in the post-peak specific rupture energy indicating rock embrittlement at failure in the post-peak region. In accordance with Wawersik and Fairhurst classification [4] negative post-peak modulus M corresponds to Class I rock behaviour, while positive M – to Class II behaviour. Increase in σ_3 can change hard rock behaviour from Class I to Class II and then to Class I again. At very high σ_3 rock behavior returns to the conventional mode. Analysis conducted in [5] showed that no one existing brittleness criteria can describe properly the variation of brittleness in this situation.

The paper proposes two new criteria [1-3,5] allowing for the representation of rock brittleness at triaxial compression within the range from absolute brittleness to absolute ductility in the form of continuous, monotonic and unambiguous scale of brittleness. Estimations of brittleness variation with rising confining stress σ_3 showed that hard rocks can become hundreds of times more brittle at highly confined conditions compared with uniaxial compression. A special shear rupture mechanism is proposed [1-3] to explain this phenomenon.

Brittleness criteria

According to classical mechanics the failure process associated with tensile crack formation is considered as brittle while shear rupture development is treated as ductile behaviour. The failure

process in rocks subjected to triaxial compression has very complicated character: macroscopically the failure zone is represented by a shear plane the structure of which on the micro-level is formed due to tensile cracks. Such dual rupture mechanism creates difficulties in determination of rock brittleness at triaxial compression. The concept of brittleness in rock mechanics is yet to be precisely defined. Below we propose new brittleness indexes which characterise degree of intrinsic macroscopic instability of rock at failure. The loss of stability can take place at the post-peak stage of the loading process only. The proposed criteria are based upon the balance between the post-peak elastic energy withdrawn from the material body at the rupture development and two other forms of post-peak energy associated with the failure process: the rupture energy and the excess (released) energy.

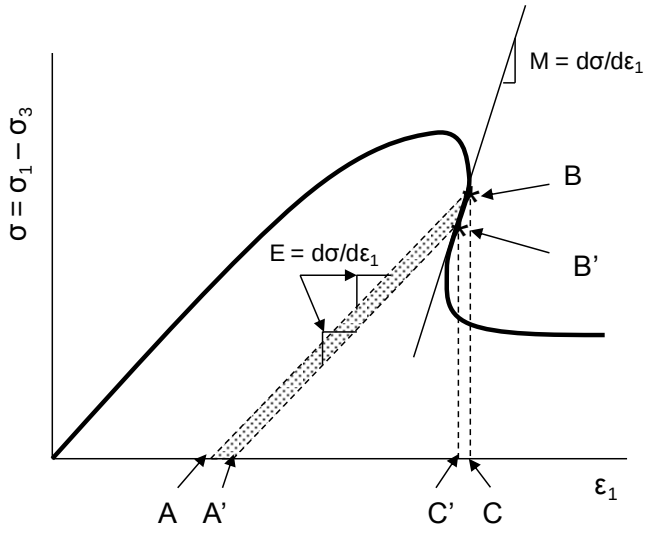

Fig.3. Principle of the current brittleness estimation by brittleness indexes K_1 and K_2.

Figure 3 shows a stress-strain curve illustrating the essence of the proposed criteria. The failure process between points B and B' is accompanied by the following variation in the energy balance. The elastic energy dW_e withdrawn from the material body is represented by the area ABCC'B'A'. The corresponding rupture energy dW_r is represented by the area ABB'A'. The area C'B'BC represents the excess (released) energy dW_a. The mentioned forms of energy can be calculated on the basis of elastic modulus E and post-peak modulus M. It is known that these modules can vary significantly with the fracture development. However, two infinitely near points located on a post-peak curve (for example points B and B') can be characterised by the same value of E, while the corresponding modulus M can be unambiguously determined on the basis of a tangent line.

Equations (1), (2) and (3) describe the mentioned above forms of energy associated with the rupture development between points B and B' in Figure 3. Equation (3) describing the post-peak rupture energy dW_r takes into account the sign of post-peak modulus M for Class I and Class II behaviour:

$$dW_e = \frac{\sigma_B^2 - \sigma_{B'}^2}{2E} \tag{1}$$

$$dW_a = \frac{\sigma_B^2 - \sigma_{B'}^2}{2M} \tag{2}$$

$$dW_r = dW_e - dW_a = \frac{(\sigma_B^2 - \sigma_{B'}^2)(M - E)}{2EM} \tag{3}$$

The brittleness index K_1 below is determined by the ratio between the post-peak rupture energy and the withdrawn elastic energy:

$$K_1 = \frac{dW_r}{dW_e} = \frac{M - E}{M} \tag{4}$$

The brittleness index K_2 represents the ratio between the excess (released) and the withdrawn elastic energy:

$$K_2 = \frac{dW_a}{dW_e} = \frac{E}{M} \tag{5}$$

Brittleness indexes K_1 and K_2 characterize unambiguously the rock brittleness at different loading conditions. Figure 4 shows scales of rock brittleness indexes K_1 and K_2 with brittleness increasing from left to right. The complete curves (differential stress σ versus axial strain ε_1) illustrate how the different curve shapes describe a variation in brittleness. It is assumed, for simplicity, that the pre-peak parts of the curves are the same. Areas defined by the large dotted triangles correspond to elastic energy W_e stored within the rock material at the peak stress, while the smaller white triangles on the right side of the curves represent the unconsumed portion of the stored elastic energy, within the material, after failure. The post-peak parts of the curves, which are characterized by the post-peak modulus M, are different for each curve. The grey areas represent the post-peak rupture energy dW_r associated with strength degradation at failure from the peak stress to the residual strength (horizontal part of the post-peak curves).

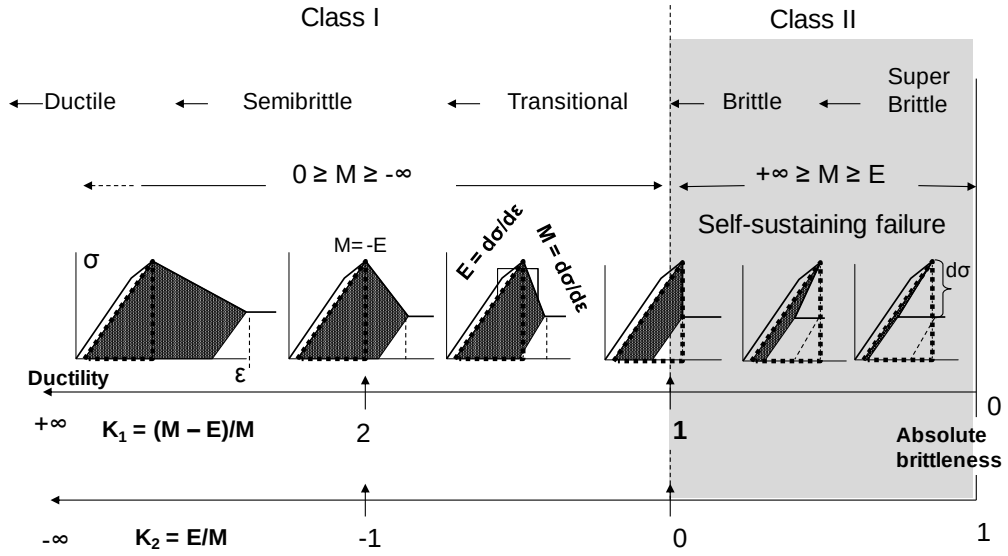

Fig.4. Scale of brittleness indexes K_1 and K_2 with characteristic shapes of complete stress–strain curves (modified from [2-3]).

Figure 4 shows variation in brittleness from absolute brittleness to ductility if read from right to left. The absolute brittleness has the following characteristics and parameters:

- The post-peak modulus is the same as the elastic modulus M = E.
- There is no portion of the stored energy transformed into post-peak rupture energy $dW_r = 0$.
- The withdrawn elastic energy is entirely transformed into excess energy $dW_e = dW_a$.
- $K_1 = 0$.
- $K_2 = 1$.

Within the range of brittleness indexes $1 > K_1 > 0$ and $0 < K_2 < 1$ the elastic energy dW_e withdrawn from the specimen material during stress degradation on the value $d\sigma$ exceeds the corresponding rupture energy dW_r, leading to self-sustaining failure (brittle Class II behaviour, shaded area). The greater the difference between dW_e and dW_r the closer the material behaviour is to absolute brittleness and the more violent is the self-sustaining failure. For the range of brittleness indexes $+\infty > K_1 > 1$ and $-\infty < K_2 < 0$ the rupture development is not self-sustaining (Class I behaviour). Variation in failure regimes corresponding to an increase in the rock brittleness is indicated in the upper part of Figure 4. These regimes are: ductile, semi-brittle, transitional, brittle and super-brittle. The characteristic features of the super-brittle regime are discussed in [2-3].

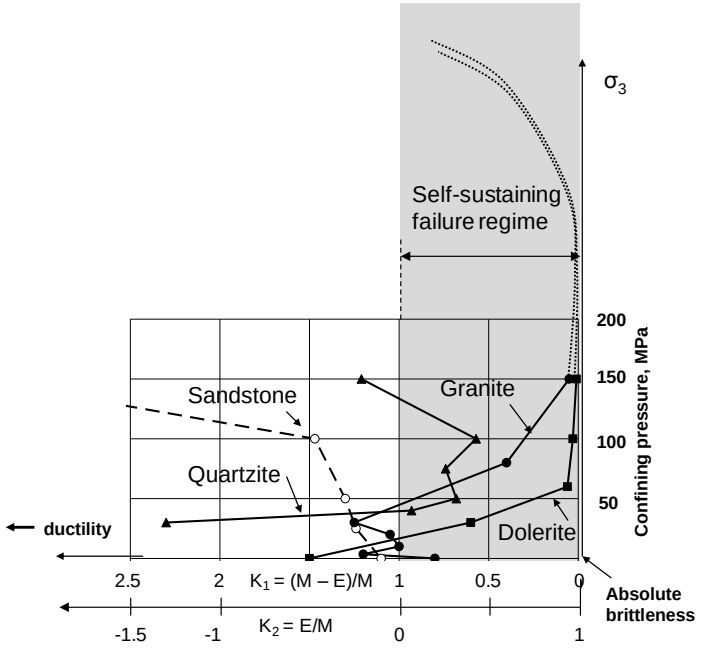

Fig.5. Variation of brittleness indexes K_1 and K_2 versus confining pressure σ_3 for rocks of different hardness (modified from [2-3]).

Figure 5 shows the variation of brittleness index K_1 and K_2 for four rocks exhibiting different responses to rising confining pressure σ_3 [2-3]. The self-sustaining failure regime corresponds to $1 > K_1 > 0$ and $0 < K_2 < 1$ (shaded area). The sandstone curve indicates that an increase in confinement σ_3 makes the rock less brittle. This behaviour is typical for softer rocks. For the quartzite, increase in confinement σ_3 within the range of 0–100 MPa makes the material more brittle. At greater confinement the brittleness decreases. The granite and dolerite show very severe embrittlement with rising σ_3. At σ_3 = 75 MPa, according to the brittleness index K_1, the dolerite became 250 times more

brittle when compared to uniaxial compression ($K_1(0) = 1.5$; $K_1(75) = 0.006$). At $\sigma_3 = 100$ and 150 MPa the brittleness increased significantly, further approaching absolute brittleness. The dotted lines indicate the expected brittleness variation for granite and dolerite at greater values of σ_3: the brittleness continues to increase until it reaches a maximum at some level of σ_3 and then decreases, as all rocks become ductile at very high confining stresses. It is estimated in [2-3] that the maximum brittleness for granite is reached at $\sigma_3 \approx 300$ MPa. For rocks that as hard as quartzite, the mode of brittleness variation is similar, but the maximum brittleness is lower and the range of confining pressure where embrittlement takes place is smaller.

Mechanism of rock embrittlement

Shear is the only form of large-scale rock failure at triaxial compression in nature and laboratory experiments. Shear rupture development represents a localized failure process. Figure 6 shows four stages of shear rupture propagation in a specimen when subjected to triaxial compression. The real shear resistance and displacement along the future failure plane are very non-uniform. Three specific zones can be distinguished (see Figure 6(ii)): (1) the process zone (or rupture head) where the failure process is in progress; (2) the core frictional zone located behind the head where the full friction is mobilized, and (3) the intact zone in front of the head where the resistance is determined by the cohesive strength. With fracture propagation the cohesive strength of decreasing zone (3) is substituted by the frictional resistance of increasing zone (2). This process is accompanied by the decrease in bearing capacity of the specimen from the cohesive strength to the frictional (residual) strength.

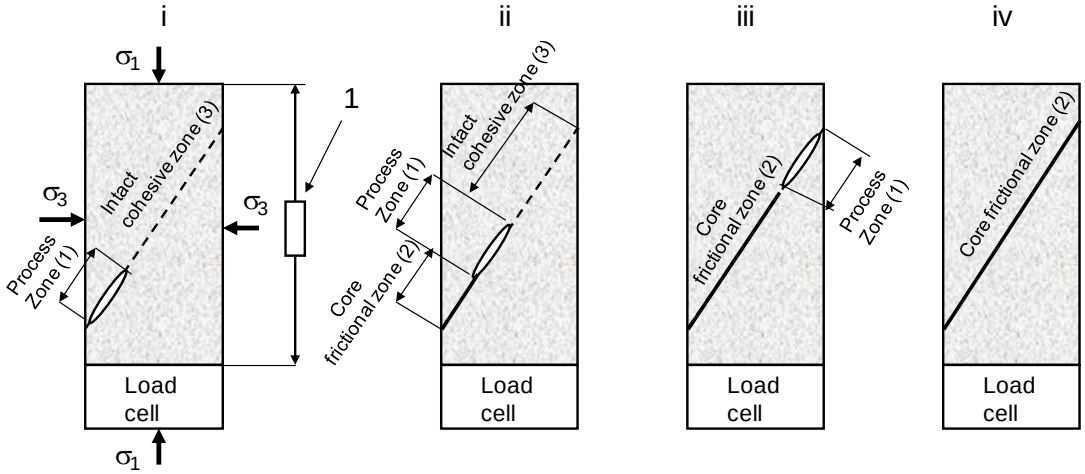

Fig.6. Four stages of shear rupture development in a specimen at triaxial compression and specific zones of shear resistance.

In common experiments the specimen is equipped with a load cell and an axial gauge 1 as shown in Figure 6(i). These gauges are capable to measure only the average load bearing capacity and the strain of the specimen during the loading procedure. On the basis of data provided by these gauges in experiments with different levels of confining stress σ_3 a set of stress σ – strain ε_1 curves can be plotted; where $\sigma = \sigma_1 - \sigma_3$ is the differential stress and ε_1 is the axial strain (see Figures 1 and 2). The development of shear rupture is mainly associated with the post-peak part of $\sigma - \varepsilon_1$ curves. The residual strength (horizontal parts of the curves) represents the frictional resistance of the completed fault (Figure 6(iv)).

It is known that a shear rupture can propagate in its own plane due to the creation of short tensile cracks in front of the rupture tips [6-8]. This forms the universal structure of shear ruptures represented by an echelon of blocks (or slabs) separated by tensile cracks – known as 'book-shelf' structure [6-10]. A model of shear rupture involving this mechanics is shown in Figure 7a. The initial angle α_0 of the tensile crack and block inclination to the shear rupture plane is about 30–40^o [11]. Shear displacement along the fault causes rotation of the blocks of the 'book-shelf' structure between the rupture surfaces [1-3,6-10].

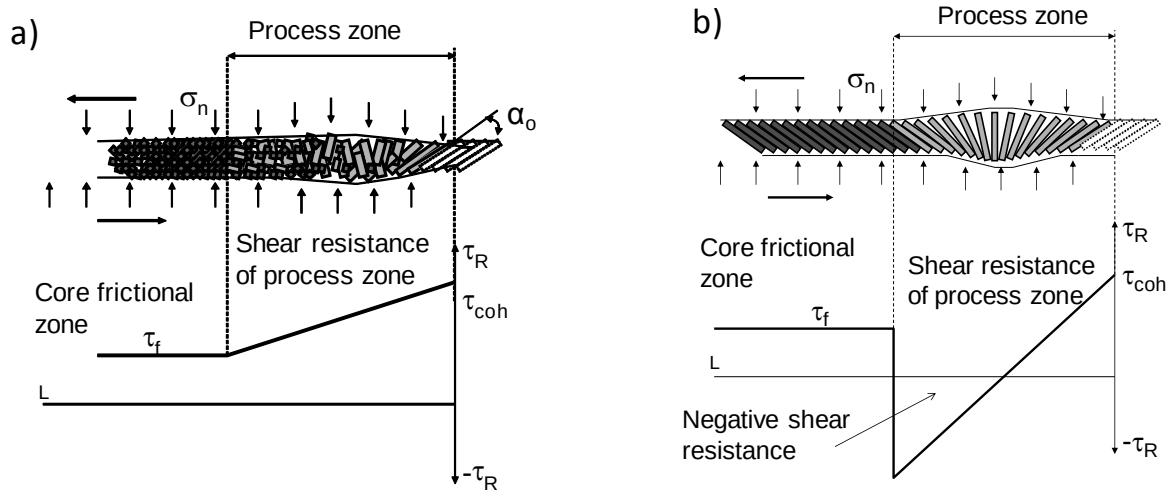

Fig.7. Illustration of rupture mechanisms at a) frictional and b) frictionless conditions of shear fracture development.

Figure 7(a) illustrates the essence of the shear rupture mechanism providing large rupture energy. Blocks located in the front part of the head create significant resistance to shear; however, they collapse with rotation providing gradual transformation of shear resistance within the head zone from cohesive to frictional levels. A graph under the shear rupture in Figure 7(a) shows the shear resistance variation along the fault head. Increase in normal (or confining) stress increases friction within the process and core zones increasing the rupture energy and making rocks more ductile. Such a rupture mechanism normally produces Class I material behaviour in the post-peak region.

Figure 7(b) illustrates a model where rotating blocks can withstand the rotation without collapse by behaving as hinges and eliminating friction between the fault surfaces. This can only happen in hard rocks because very strong material is required to achieve this (see details in [1-3]). Due to consecutive formation and rotation of the blocks, these should form a fan structure within the rupture head. A remarkable feature of the rotating blocks (hinges) in the second half of the fan structure (where $\beta > 90°$) is the creation of active forces under the effect of normal stress applied. A graph under the shear rupture in Figure 7(b) shows the shear resistance variation along the fault head. The bottom part of the graph represents active forces (negative resistance) acting in the second half of the head and assisting the fault displacement. In the core zone represented by blocks that have completed their rotation the normal residual friction is restored.

The fan structure represents a self-equilibrating mechanism and can move spontaneously as a wave with very small shear resistance. In the idealised fan-head model, the resistance to rupture propagation is determined only by the tensile strength of the material associated with consecutive formation of tensile cracks (and blocks between them) in front of the propagating rupture. It is important that the fan head can propagate independently of the core zone, which can remain

immobile due to high frictional resistance at high levels of confining stress σ_3. This mechanism creates conditions for a pulse-like mode of fracture propagation. In this situation the rupture energy is determined by shear resistance of the fan head only. The fan-head rupture mechanism represents the most energy efficient shear rupture mechanism. This mechanism is responsible for Class II behaviour with extremely small rupture energy.

The brittleness variation with rising σ_3 shown in Figure 5 for hard rocks can be explained as follows. The efficiency of the frictionless mechanism is determined by how perfect and uniform the fault structure is. It is known that increase in σ_3 decreases the tensile crack length and consequently the block length. At low levels of σ_3, when the relative length (length/thickness) of the rotating block is large, the blocks are subjected to partial destruction (buckling) as they rotate. At higher σ_3, with shorter blocks, this imperfection decreases, rendering the frictionless mechanism more efficient. The optimal efficiency takes place when the blocks rotate with minimum destruction making the material ultimately brittle. At greater σ_3 the efficiency reduces because shorter blocks gradually lose any potential for creating negative resistance from rotation. Finally very short blocks lose this capability completely and the rock behaviour returns to the commonly accepted frictional mode.

Conclusions

We can conclude that:

- Fracture mechanisms operating within the process zone play the key role in the character of transformation from the cohesive to frictional strength which determines the shape of post-peak curves, the post-peak rupture energy and stability of the failure process (or rock brittleness).
- The proposed frictionless rupture mechanism can provide the dramatic rock embrittlement under the effect of rising confining stress within a certain range of σ_3.
- Two new brittleness criteria allow for the representation of rock brittleness at triaxial compression within the range from absolute brittleness to absolute ductility in the form of continuous, monotonic and unambiguous scale of brittleness.

References

[1] B. G. Tarasov and M.F. Randolph: Int. J. Rock Mech. Min. Sci. Vol. 45, (2007), pp. 316-328.
[2] B.G. Tarasov. Superbrittleness of rocks at high confining pressure, in: Fifth International Seminar on Deep and High Stress Mining, (2010), pp. 119-133.
[3] B.G. Tarasov and M.F. Randolph: Int. J. Rock Mech. Min. Sci. Vol. 48, (2011), pp. 888-898.
[4] W.R.Wawersik and C. Fairhurst: Int. J. Rock Mech. Min. Sci. Vol. 7 (1970), p.561-75.
[5] B.G. Tarasov and Y. Potvin, in: Sixth International Seminar on Deep and High Stress Mining, (2012), pp. 313-324.
[6] Z. Reches: EPSL, (1999), Vol. 170, pp. 475-86.
[7] S.J.D. Cox and C.H. Scholz: J. Struct. Geol. (1988), Vol. 10, pp. 413-30.
[8] Z. Reches and D.A. Lockner: J. Geophys. Res. (1994), Vol. 99, No. B9, pp. 18159-73.
[9] S. Peng and A.M. Johnson: Int. J. Rock. Mech. Min. Sci. (1972), Vol. 9, pp.37-86.
[10] G.C.P. King and C.G. Sammis: PAGEOPH (1992), Vol. 138, 4, pp.611-40.
[11] H. Horii and S. Nemat-Nasser: J. Geophys. Res. (1985), Vol. 90, pp.3105-25.